Proceedings of the ASME 2020 39th International Conference on Ocean, Offshore and Arctic Engineering
OMAE2020
August 3-7, 2020, Virtual, Online

OMAE2020-19071

ON THE STABILITY OF OIL-BASED DRILLING FLUID: EFFECT OF OIL-WATER RATIO

Titus Ntow Ofei[1], Itung Cheng[2]
Norwegian University of Science and Technology[1]
The City College of New York[2]

Bjørnar Lund[3], Arild Saasen[4], Sigbjørn Sangesland[1]
SINTEF[3]
University of Stavanger, Norway[4]

ABSTRACT

Drilling fluids are complex mixtures of natural and synthetic chemical compounds used to cool and lubricate the drill bit, clean the wellbore, carry drilled cuttings to the surface, control formation pressure, and improve the function of the drill string and tools in the hole. The two main types of drilling fluids are water-based and oil-based drilling fluids, where the oil-based also include synthetic-based drilling fluids.

Many rheological properties of drilling fluids are key parameters that must be controlled during design and operations. The base fluid properties are constructed by the interaction of the emulsified water droplets in combination with organophilic clay particles. The rheological properties resulted from this combination, along with the particle size distribution of weight materials are vital in controlling the physical stability of the microstructure in the drilling fluid. A weak fluid microstructure induces settling and sagging of weight material particles. The presence of sag has relatively often been the cause for gas kicks and oil-based drilling fluids are known to be more vulnerable for sag than water-based drilling fluids. Hence, the shear-dependent viscosity and elasticity of drilling fluids are central properties for the engineers to control the stability of weight material particles in suspension.

In this study, we examined the stability of typical oil-based drilling fluids made for North Sea oilfield drilling application with oil-water-ratios (OWR) of 80/20 and 60/40. The structural character of the fluid samples was analyzed both at rest and dynamic conditions via flow and viscosity curves, amplitude sweep, frequency sweep, and time-dependent oscillatory sweep tests using a rheometer with a measuring system applying a grooved bob at atmospheric conditions. A high precision density meter was used to measure the density of the drilling fluid samples before and after each test. The measurement criteria used to rank the fluids stability include the yield stress as measured from flow curves and oscillatory tests, flow transition index, mechanical storage stability index, and dynamic sag index.

We observed that between the two drilling fluids, the sample with OWR = 60/40 showed a stable dispersion with stronger network structure as evidenced by higher yield stress and flow transition index values, while the mechanical storage stability index and dynamic sag index recorded lower values. The results of this study enable drilling fluid engineers to design realistic oil-based drilling fluids with stable microstructure to mitigate settling and sagging of weight material particles for North Sea drilling operation.

Keywords: Oil-based drilling fluid, Stability, Rheology, Viscoelasticity, Gas kick, Oil-water ratio, Barite sag.

NOMENCLATURE

DSI	dynamic sag index (-)
FTI	flow transition index (-)
LVE	linear viscoelastic range
$MSSI$	mechanical storage stability index (-)
OWR	oil-water-ratio (-)
G^*	complex shear modulus (Pa)
G'	storage modulus (Pa)
G''	loss modulus (Pa)
δ	phase shift angle (^{o})
τ	stress (Pa)
τ_A	stress amplitude (Pa)
τ_f	flow stress (Pa)
τ_y	dynamic yield stress (Pa)
τ_s	static yield stress (Pa)

[1] Contact author: titus.n.ofei@ntnu.no / titusofei@hotmail.com

$\dot{\gamma}$	shear rate (1/s)
γ_A	strain amplitude (%)
η^*	complex viscosity (Pa s)
ρ_{sag}	dynamic sag density (g/cm^3)
$\rho_{initial}$	initial density (g/cm^3)
ρ_{final}	final density (g/cm^3)

INTRODUCTION

Drilling operations often result in the settling of weighting materials in the drilling fluids which may cause several problems. These problems range from difficulty in running of casing, insufficient displacement efficiency during cementing operation, fracturing of formation when re-suspending a weight material bed, insufficient drilling fluid volume for well control, and stuck pipes [1 – 4]. The term 'barite sag' is a generic description of the settling of suspended weight material particles in drilling fluids. Barite as used by the oil industry is an impure mined grade of Barium Sulphate with a minimum specific gravity (sg) of 4.2. The particle size specifications for the ground ore are less than 30% by weight below 6 microns and less than 3% by weight greater than 75 microns [5]. Sag of suspended barite particles occurs both during static and dynamic drilling conditions. Whereas static sag is influenced by the rheological properties of the fluid, particle density, shape, size, concentration and structural strength of the network, dynamic sag is mainly affected by shear rate of the flow regime, hole size, hole angle, drill pipe eccentricity and drill pipe rotational speed [5 – 9].

The presence of sag has relatively often been the cause for gas kicks and oil-based drilling fluids are known to be more vulnerable for sag than water-based drilling fluids. The composition of oil-based drilling fluids is complex and comprise of internal brine phase, mineral oil, surfactants to emulsify the internal phase, organophilic clays as rheology modifiers, lime to saponify free fatty acids and to act as a buffer to acid gas intrusion, barite to increase the fluid density, and supplementary additives to reduce filtration and increase or decrease rheological parameters. Several studies have outlined some factors that can influence the stability of oil-based drilling fluids under both static and dynamic sag conditions. The properties of barite particle have shown to influence sag. Under both static and dynamic sag conditions, minimum sag is achieved with barite with d_{50} of 3 microns or less, however, formulated drilling fluids with coarser barite material significantly increase the risk of barite sag [10].

Drilling fluid additives have been observed to have impact on sag. Drilling fluids containing polymeric "*modifiers*" resulted in higher barite sag than fluids containing organophilic clays especially under dynamic conditions [3, 4, 11, 12]. Modifiers are hydrophobic polymers with hydrophilic ends that bridge off two nearby droplets. The authors attributed this behaviour to the low-shear-rate (LSR) viscosity, and the absence of network structure made by these polymeric additives in the drilling fluids. On the contrary, Elkatatny [13] observed that addition of copolymers, consisting of styrene and acrylic monomers, eliminated sag potential under both static and dynamic conditions. Additionally, excess oil wetting surfactants on organophilic clays produces syneresis, thereby increasing sag potential in both static and dynamic conditions with time [5]. Combining different weighting materials is known to influence sag in oil-based drilling fluids. A critical concentration of 40 wt.% of ilmenite added to barite was enough to eliminate sag in both static and dynamic conditions [14]. This is attributed to the surface charge and the size of solid particles [15]. It is also observed that increasing the oil-water-ratio (OWR) of the drilling fluid reduces the viscosity, thus promoting sag effect [16].

Effect of drilling parameters were also addressed on barite sag performance. Increasing annular velocity is the most significant impact on preventing barite sag. Inclination angles in the range from 45º to 60º from vertical give highest risk for barite sag. Furthermore, an eccentric drill pipe induces more sag than a concentric one, due to the lower fluid velocities in the narrow part of the annulus. However, drill pipe rotation prevents barite sag better in eccentric annulus than in concentric annulus [9, 10, 12].

Fluid properties also play important role on the sag potential in oil-based drilling fluids. It is believed that with higher viscosity, less dynamic sag is observed [6, 17 – 19]. However, it may be concluded that building fluid viscosity does not directly equate to prevention of the settling of weight material [20], an issue previously addressed with the general conclusion that clay viscosifiers, which better produce structure, are more effective at managing barite sag in oil-based drilling fluids than polymeric viscosifiers [4, 21]. For static suspension of weight materials, high gel strength is necessary, however, the benefits of elevating the gel strength is not observed in dynamic condition [1]; [6]; [19]. Yield stress also plays a very important role in keeping the barite particles in suspension under static condition. It is reported that the settling of barite particles will not occur if the yield stress is higher under static condition [9]. It is also noted that there is a possible connection between the dynamic yield stress and dynamic sag as examined from the structural stability of field drilling fluid [12].

In this study, we discussed the stability of two oil-based drilling fluids made for North Sea Oilfield drilling application with oil-water-ratios (OWR) of 80/20 and 60/40 under both static and dynamic conditions. The stability criteria used include yield stress, flow transition index, mechanical storage stability index, and dynamic sag index.

MATERIALS AND METHOD

1.1 Fluid Composition

The drilling fluid is a referenced standard oil-based fluid (OBDF) with oil-water ratios of 80/20 and 60/40. The fluid components were supplied by M-I Swaco, Schlumberger in Norway, and consists of a refined mineral oil as base fluid of density and kinematic viscosity as 814 kg/m^3 and 5.9 mm^2/s respectively at 20ºC, brine of calcium chloride, lime, emulsifier, organophilic clay viscosifiers, fluid loss agent, low gravity calcium carbonate, and API barite. A Hamilton Beach mixer is

used to mix the components of the drilling fluid at a speed of 6000 rpm for a total of 70 minutes. Table 1 shows the various components of the drilling fluid including their mass fraction, concentration, and mixing time. A constant 1.43 g/cm^3 of drilling fluid density was formulated.

TABLE 1: Components of the 1.43 g/cc oil-based drilling fluid (OBDF)

	OWR = 80/20		OWR = 60/40		
Product	Mass fraction	Concen-tration (g/l)	Mass fraction	Concen-tration (g/l)	Mixing time (min.)
Refined mineral oil	0.35	501.9	0.26	378.9	-
Emulsifier	0.0139	20.0	0.0139	20.0	2
Viscosifier (low temp. clay)	0.00628	9.0	0.00628	9.0	4
Viscosifier (high temp. clay)	0.00907	13.0	0.00907	13.0	4
Lime	0.0139	20.0	0.0139	20.0	5
Fluid loss agent	0.00697	10.0	0.00697	10.0	5
Calcium chloride brine	0.139	199.3	0.274	391.2	15
Calcium carbonate	0.0349	50.0	0.0349	50.0	10
API barite	0.426	610.8	0.376	538.2	25

1.2 Fluid Mixing Procedure

Pour the base oil in a container and place the container in ice water bath to maintain the fluid's temperature below 65ºC. The use of a cooling bath is not necessary until the temperature exceeds 55ºC. It should be noted that some of the fluid products require the initial heat to better solute in the base oil and to be fully activated. The base oil is poured into the Hamilton beach container and the emulsifier added and mixed for 2 minutes. The low temperature and high temperature viscosifiers are then added to the mixing container in sequence and mixed for 4 minutes apart. Afterwards, the lime is added and mixed in the container for 5 minutes, followed by the fluid loss agent which is also mixed for 5 minutes. The brine of calcium chloride is then added and mixed for 15 minutes which is then followed by the addition of the API barite and mixed for 25 minutes. The calcium carbonate is finally added to the mixture and mixed for 10 minutes to act as bridging material to strengthen the fluid loss properties and minimize filter cake thickness, especially in permeable formation.

The final density of the drilling fluid sample was measured to be 1.43 g/cm^3. Two sets of fluid samples of oil-water ratios of 80/20 and 60/40 compositions were mixed and preconditioned at atmospheric temperature and pressure.

1.3 Fluid Characterization

A rheometer, Anton Paar MCR 302 using a Couette geometry with grooved bob was utilized to conduct the rheological measurements on the OBDF at 25ºC. The various rheological tests performed include, flow curves, oscillatory amplitude sweep, oscillatory frequency sweep, and tests at constant rotational and oscillatory shear rates.

The flow curves were measured with controlled shear rate and show the viscosity function of the sample. We pre-sheared the sample at a constant shear rate of 1022 s^{-1} for 300 s before linearly ramping down the shear rate from 1022 to 1.0 s^{-1} for 100 measuring points with 5 s measuring point duration. Then, the shear rate was logarithmically ramped down from 1.0 s^{-1} to 0.001 s^{-1} for 40 measuring points with 4 s measuring point duration to capture the flow characteristics in the low shear rate region. In a similar manner, the shear rate was ramped up logarithmically from 0.001 s^{-1} to 1.0 s^{-1} for 40 measuring points with 4 s measuring point duration and then linearly ramped up from 1.0 s^{-1} to 1022 s^{-1} for a total of 100 measuring points with 5 s measuring point duration. A difference between the ramping down and ramping up flow curves indicate a thixotropy behavior of the sample. The present study reveals insignificant difference between the flow curves.

The amplitude sweep tests which uses sinusoidal oscillations allows the testing of the microstructure of the sample without breaking the sample structure [18]. The test was carried out with a constant angular frequency of 10 rad/s and increasing strain amplitude from 0.001 to 100% at a slope of 5 measuring points per decimal, accounting to 26 measuring points. The limit of the linear viscoelastic (LVE) range, below which the measured properties of the sample are non-destructive, is determined for use as a parameter for the frequency sweep test. The test also measures the storage modulus (G'), characterizing the material's elastic behavior, and loss modulus (G''), characterizing the viscous behavior of the material. The flow point, where $G' = G''$, is measured as the point where the material's microstructure deforms and initiates flow. If $G' > G''$, the elastic behavior dominates the viscous behavior and the sample depicts a solid-like character. Conversely, $G'' > G'$, indicates that the viscous behavior dominates the elastic behavior of the sample and shows a liquid-like character.

By oscillatory shear test, certain parameters have been adopted from classic mechanics to measure the rheological properties of the viscoelastic fluid. The shear modulus G, under uniaxial stress conditions, according to Hooke's law, is constant for perfectly elastic material. However, for oscillatory stresses, a complex shear modulus, G^*, which is divided into a storage modulus, G', and a loss modulus, G'', is defined by the following equations [22],

$$G^* = \frac{\tau_A}{\gamma_A} \tag{1}$$

$$G' = |G^*|\cos(\delta) = \left|\frac{\tau_A}{\gamma_A}\right|\cos(\delta) \tag{2}$$

$$G'' = |G^*|\sin(\delta) = \left|\frac{\tau_A}{\gamma_A}\right|\sin(\delta) \tag{3}$$

where τ_A in (Pa), is the stress amplitude, γ_A (%) is the strain amplitude, and δ is the phase shift angle between G'' and G'.

The frequency test also uses sinusoidal oscillations at small strain amplitudes usually within the LVE range [18]. A shear strain amplitude within the LVE range was applied on the sample over a decreasing range of angular frequency from 100 to 0.001 rad/s at a slope of 5 measuring points per decimal, amounting to 26 measuring points. The comparison of $G'$and G'' is of greater importance at lower frequencies where dynamic sag is more likely to occur. From $G'$and G'' we calculate the phase shift angle, δ, of the sample, which is defined by $\tan(\delta) = G''/G'$, which is also called the damping factor. The phase shift angle and the damping factor characterizes the viscoelastic behavior of the sample, where $\delta = 0°$ corresponds to ideal elastic solid behavior and $\delta = 90°$corresponds to purely viscous liquid behavior. Thus, the sample is more viscous when $\tan(\delta) > 1$, and more elastic when $\tan(\delta) < 1$ [4].

During the steady time test, the viscosity of the sample was measured at a constant shear rate in isothermal condition (25ºC) for a fixed length of time. The constant shear rates used are10.22, 5.11, 1.7, 0.60, 0.10, 0.01, and 0.001 s^{-1}. The duration and the number of measurement points were 10,800 s and 1000, respectively, per shear rate.

For dynamic time test, both strain amplitude and angular frequency were held constant. Angular frequencies from 10.22 – 0.001 rad/s and strain amplitude of 0.05% and 5% were imposed and each experiment was run for a total time of 10,800 s at 1000 measuring points with 4 s interval. An isothermal condition of 25ºC was imposed.

1.4 Barite Sag Test

The testing of the dynamic barite sag of the fluid sample was carried out using the Anton Paar rheometer MCR 302 and Anton Paar density meter DMA 5000 M. After mixing the fluid components, its initial density, $\rho_{initial}$, was measured using the digital density meter DMA 5000 M with a tolerance of $\pm 5 \times 10^{-5}\ g/cm^3$. It is based on a U-tube principle which measures the inertial mass of a known sample volume. The fluid sample is filled into a U-shaped tube that is mounted on a countermass using a syringe. The U-tube is then excited and starts to oscillate. The change in frequency is then measured and the density can be determined [23]. The instrument performs several measurements automatically. Before the rheometer measurements, the initial density, $\rho_{initial}$ of the fluid sample is measured after pre-shearing for 2 minutes with the Hamilton Beach mixer. The final density, ρ_{final} of the sample is however measured after the rheometer measurements at both steady rotational shear and oscillatory shear conditions after a period of 10,800 s. For a single sample injection into the density meter, three series of measurements were taken after which the average value of these measurements was calculated.

The grooved bob-in-cup measuring system of the Anton Paar rheometer MCR 302 was used to investigate the dynamic barite sag of the fluid sample at a constant temperature of 25ºC. Drilling fluid sample of ~20 mL was poured into the measuring cup. Both steady rotational shear and oscillatory shear conditions were imposed where for each fixed shear rate or frequency, the apparent viscosity or complex viscosity was measured over a time period of 10,800 s. At the end of each run, ~3 mL of the fluid sample was taken from the top of the measuring cup using a syringe and its density, ρ_{final}, measured using the density meter. The complex viscosity, η^*, which defines the viscoelastic flow resistance of the sample is expressed as [22]:

$$\eta^* = \frac{\tau(t)}{\dot{\gamma}(t)} \tag{4}$$

where $\tau(t)$ and $\dot{\gamma}(t)$ are the complex stress and shear rate respectively.

1.5 Stability Criteria

The presence of a yield stress, τ_y, means that the material starts to flow only under the action of an applied shear force. The applied force must be higher than the internal forces of the material structure at rest. The term dynamic yield stress refers to a quantity measured under dynamic conditions where a constant or time-varying shear rate is applied. This quantity is therefore process related. The dynamic yield stress can be measured more accurately from the amplitude sweep where the yield stress of the material is determined as the shear stress where $G' = 0.9G'_{lin}$ (see Figure 4). So long as the stresses below the yield stress are applied, no significant change of the internal structure could occur, hence, the sample would show reversible viscoelastic behavior. A higher yield stress fluid indicates a high suspension capability of the fluid sample. On the other hand, a static yield stress, τ_s represents the shear stress required to make a material at rest to start flowing after a required time. Static yield stress is only dependent on the time of the measurement and represents the shear stress where the material changes from its solid state to liquid state. A more accurate measuring method for measuring static yield stress is creep test where a constant stress is applied to a material as a function of time and a deformation as a function time of the material can be measured.

We define the flow transition index, $FTI = \tau_f/\tau_y$, as a ratio of flow stress to dynamic yield stress to characterize the breaking behaviour of the inner structure. This parameter is indicative of the ability of the structure to yield, breakdown and similarly to rebuild. Thus, a lower FTI value indicate a stiff and brittle fluid sample whereas a high value shows a dense network structure.

The mechanical storage stability index, $MSSI$, measures the deformation stability and time behavior of the fluid structure in the region of the long-term (low frequency) behavior. The $MSSI$ can be defined from the slope of G' curve in the long-term region from a frequency sweep test. Thus:

$$MSSI = \frac{G'(1.0\ s^{-1})}{G'(0.1\ s^{-1})} \tag{5}$$

A lower value of $MSSI$ indicates a more stable fluid suspension while a higher $MSSI$ value shows separation of the dispersed phase in the fluid sample.

The dynamic sag density, ρ_{sag} and dynamic sag index, DSI, are respectively defined as:

$$\rho_{sag} = \rho_{initial} - \rho_{final} \tag{6}$$

$$DSI = \frac{\rho_{initial}}{2\rho_{final}} \tag{7}$$

For a fluid to exhibit perfect suspension characteristics, the DSI should be 0.50. A fluid which has a DSI greater than 0.53 is considered to have inadequate suspension properties [12]. It should be noted that DSI values less than 0.50 might be measurement errors but could also imply negative sag, which might occur for nanoparticles or by flotation if certain gases are dissolved. In this study, a DSI greater than 0.51 is considered as the region vulnerable to sag, whereas DSI less than 0.51 indicate a favorable sag region.

RESULTS AND DISCUSSION

Flow and Viscosity Curves

The flow characteristic and viscosity curves of the fluid samples with OWR of 80/20 and 60/40 are presented in Figure 1. The dynamic viscosity increased over the entire range of shear rate for fluid sample with OWR = 60/40 compared to fluid sample with OWR = 80/20. The behavior of both fluid samples shows a shear-thinning effect with a monotonous decreasing viscosity profiles as shear rate increased. The graph is linear between 0.001 s^{-1} and 10 s^{-1} indicating a power-law region, whereas, a gradual transition towards a quasi-Newtonian region exists between 10 s^{-1} to 1022 s^{-1}.

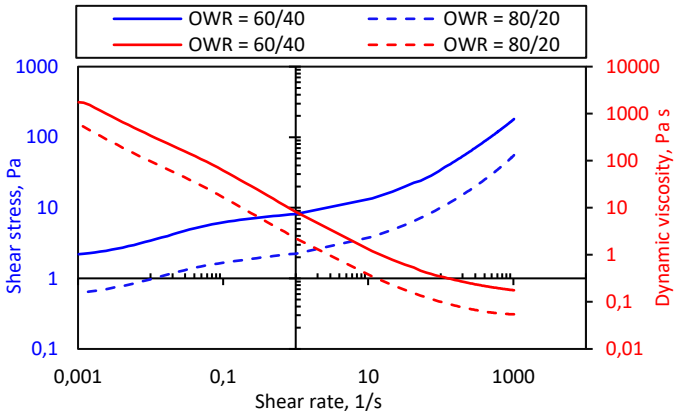

FIGURE 1: Flow and viscosity profiles between drilling fluid samples with OWR of 80/20 and 60/40 measured at 25°C

Amplitude Sweep

From Figure 2, the structural character of both fluid samples show that the elastic behavior dominates the viscous behavior, i.e., $G' > G''$, exhibiting a gel-like character in the linear viscoelastic (LVE) range, and a liquid-like character beyond the flow point ($G' = G''$) where the viscous behavior dominates the elastic one. The G' and G'' curves maintained a constant plateau values below the limit of LVE range for both fluid samples. This indicates that the structure of both fluid samples shows no significant change at these low deformations. However, the value of G' for fluid sample with OWR = 60/40 exceed that of fluid sample with OWR = 80/20 by a factor of more than 5, an indication of higher elastic behavior of fluid sample with OWR = 60/40. Three distinct zones exist which are: (a) the LVE range where $G' > G''$ with gel-like structural character, (b) the yield zone between the limit of LVE and flow point, where still $G' > G''$, however the reversible-elastic deformation range is exceeded and therefore irreversible behavior is present, and (c) the liquid-like structural character where $G'' > G'$.

The yield zone shows a slight peak in G" curve for the fluid sample with OWR = 60/40. This can be interpreted that the structural network of the fluid sample does not collapse suddenly in the whole shear gap if the LVE range has been exceeded. It begins with the forming of micro-cracks which grow into macro-cracks until the G''-peak is exceeded, and finally a large crack divided the entire shear gap.

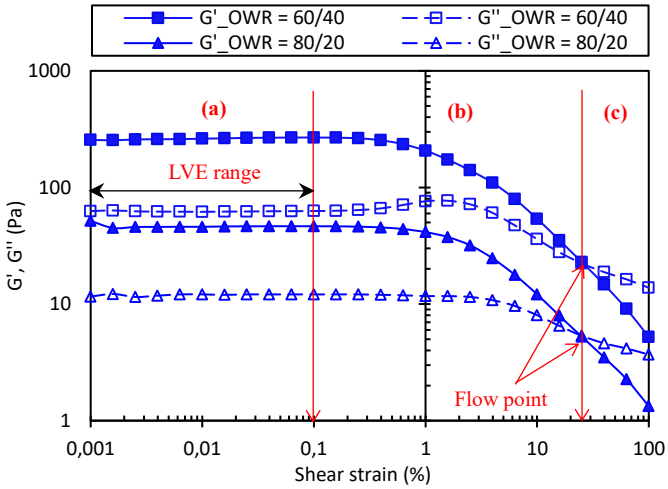

FIGURE 2: Amplitude sweep comparing drilling fluid samples with OWR of 80/20 and 60/40 measured at 25°C presented with shear strain showing the limit of LVE range and flow point at $G' = G''$ at frequency of 10 rad/s

In Figure 3, shear strain is plotted versus shear stress, obtained from amplitude sweep tests. For the fluid sample with OWR = 60/40, the dynamic yield stress value is approximately 3.5 times that of fluid sample with OWR = 80/20. Likewise, the flow stress value increased more than 4 times for fluid sample with OWR = 60/40 compared to fluid sample with OWR = 80/20. This is an indication of high amount of water droplets in the fluid sample with OWR = 60/40, causing structural strengthening and resulting to a denser network leading to higher rigidity. For fluid sample with OWR = 80/20, the dynamic yield stress value measured as the stress at $G' = 0.9G'_{lin}$ from the

amplitude sweep is 0.4 Pa at shear strain of 0.94% and a flow stress of 1.9 Pa measured at $G' = G''$ Similarly, fluid sample with OWR = 60/40 recorded a dynamic stress of 1.4 Pa measured as the stress at $G' = 0.9G'_{lin}$ from the amplitude sweep at shear strain of 0.5% and a flow stress of 8.2 Pa measured at $G' = G''$. The flow transition index, $FTI = \tau_f/\tau_y$ calculated for both fluid samples with OWR of 80/20 and 60/40 are 4.8 and 5.9 respectively. This shows a dense structural network in the fluid sample with OWR = 60/40 whereas OWR = 80/20 fluid sample reveals a stiff and brittle network. For more clarity, the dynamic yield stress is evaluated from Figure 4, where the storage modulus is plotted against the shear stress from the amplitude sweep tests on a semi-log axis.

Figure 5 shows a creep measurement with a constant applied shear stress to obtain the static yield stress, τ_s. The fluid samples are considered to flow under a constant shear stress if the shear rate is higher than $0.01s^{-1}$ at 60 s. The static yield stress value of fluid sample with OWR = 80/20 is found to be 5 Pa whiles for the fluid sample with OWR = 60/40, the static yield stress is 10 Pa.

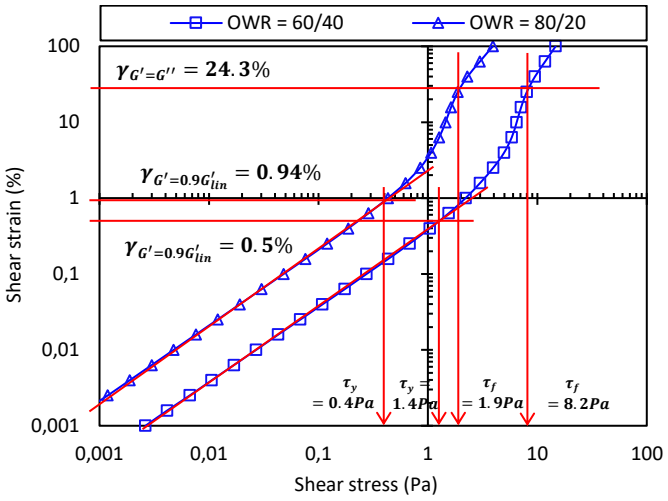

FIGURE 3: Shear strain vs shear stress comparing drilling fluid samples with OWR of 80/20 and 60/40 measured at 25ºC. The dynamic yield stress, τ_y and flow stress, τ_f values correspond to the shear stress values at $G' = 0.9G'_{lin}$ and $G' = G''$ respectively at frequency of 10 rad/s

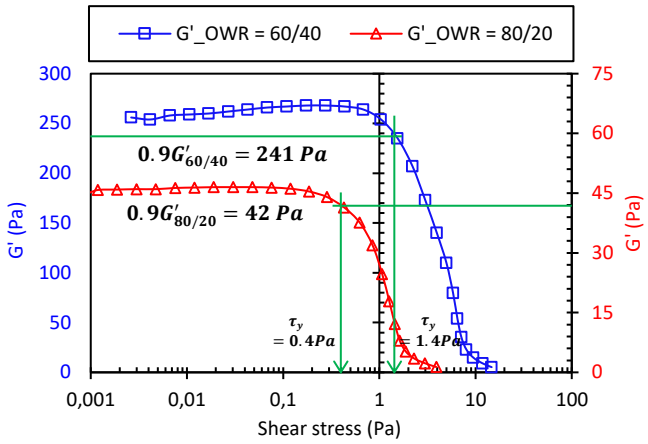

FIGURE 4: Storage modulus vs shear stress comparing drilling fluid samples with OWR of 80/20 and 60/40 measured at 25ºC. The dynamic yield stress, τ_y values correspond to the shear stress values at $G' = 0.9G'_{lin}$ at frequency of 10 rad/s

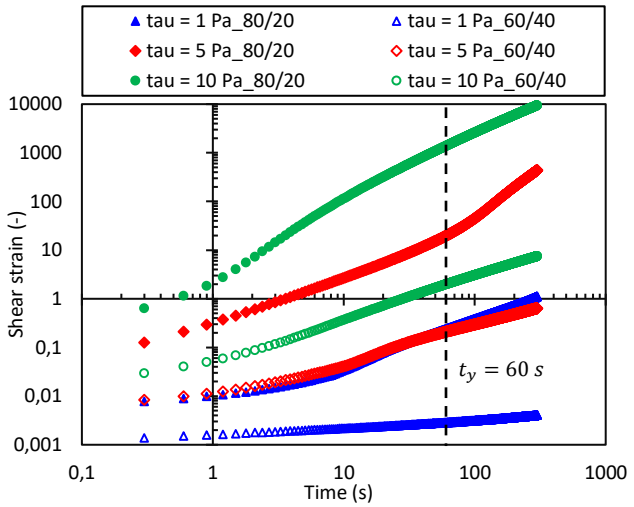

FIGURE 5: Creep test for determining static yield stress comparing drilling fluid samples with OWR of 80/20 and 60/40 measured at 25ºC. The static yield stress values correspond to the applied shear stress at the shear rate reached $0.01s^{-1}$ at 60 s

Frequency Sweep

Figure 6 shows the time-dependent deformation behaviour of the fluid samples structure within the LVE range of shear strain. Both fluid samples show weak gel structure with $G' > G''$ and in parallel over the whole frequency range, therefore exhibiting a gel-like structure and physical long-term stability at rest. A weak gel arises when the material has an infinite viscosity, while at the same time having a vanishing equilibrium shear modulus [24]. The G' values for the fluid sample with OWR = 60/40 are however 5 times higher than for the fluid sample with OWR = 80/20. This is due to higher water droplet concentration creating a more stable crystalline structure. Such a structure will create a high but extremely brittle elasticity. Furthermore, both fluid samples show complex viscosities sloping up towards high values in the range of low frequencies

due to high degree of cross-linked molecules. The mechanical storage stability index, $MSSI$, calculated from the slope of G' in the low frequency (long time) region for both fluid samples are 1.3 and 1.2 for OWR = 80/20 and OWR = 60/40 respectively. This indicates a much more stable suspension of fluid sample with OWR = 60/40 compared to fluid sample with OWR = 80/20, since $MSSI_{60/40} < MSSI_{80/20}$.

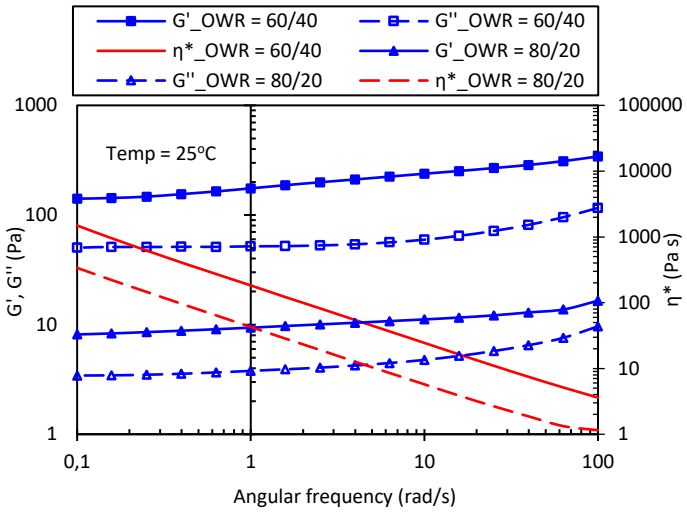

FIGURE 6: Frequency sweep test comparing drilling fluid samples with oil-water ratio (OWR) of 80/20 and 60/40 measured at 25°C showing the viscous and elastic moduli as well as complex viscosity at LVE value of 0.05%.

Time-Dependent Oscillatory Sweep

Figure 7 shows the time-dependent behavior of G' and G'' curves at constant dynamic-mechanical and isothermal conditions. The strain value was chosen between the strain values corresponding to the yield stress and flow stress in the amplitude sweep test (see Figure 2) where the latter causes an irreversible deformation of the structure of the sample. In both fluid samples, $G' > G''$ up to approximately 1600 s and 2400 s for fluid samples with OWR = 60/40 and 80/20 respectively, indicating a gel-like character. Beyond the flow points, a viscoelastic liquid behavior exists as $G'' > G'$. The decrease in G' curves show a decreasing structural strength due to molecular disentanglement as a result of decreasing interactive forces of polymers and dispersions. In Figure 8, however, the strain value is chosen within the LVE range where the fluid structure is stable. Here, we also see $G' > G''$, indicating gel-like structures and physical stability for both fluid samples. Fluid sample with OWR = 60/40 shows a continuous increasing structural strength due to molecular entanglements over the time range. For the fluid sample with OWR = 80/20, there is initial structural growth up to 3600 s, while afterwards a structural breakdown is observed due to decreasing interaction forces, thus causing a separation of the barite particles in the fluid sample. This test also shows the critical time below which the fluid sample remains stable. It is evidenced that after 3600 s the fluid sample with OWR = 80/20 becomes unstable with respect to barite sag.

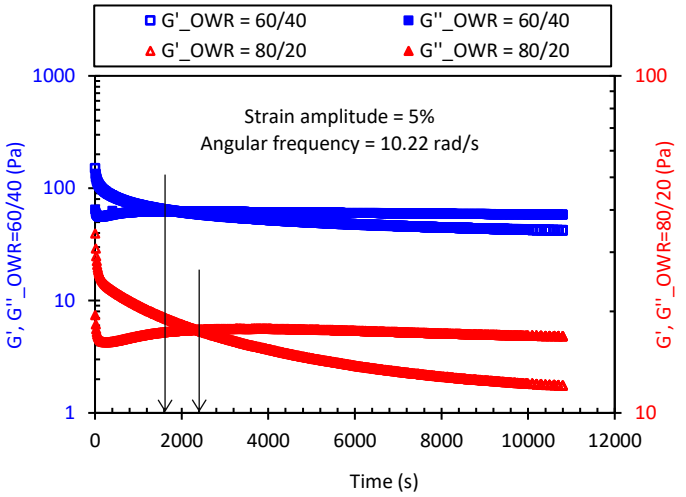

FIGURE 7: Time-dependent oscillatory shear analysis of drilling fluid sample with oil-water ratio (OWR) of 80/20 and 60/40 showing the characteristic profiles of the elastic and viscous moduli in the yield zone at amplitude strain of 5% and angular frequency of 10.22 rad/s measured at 25°C.

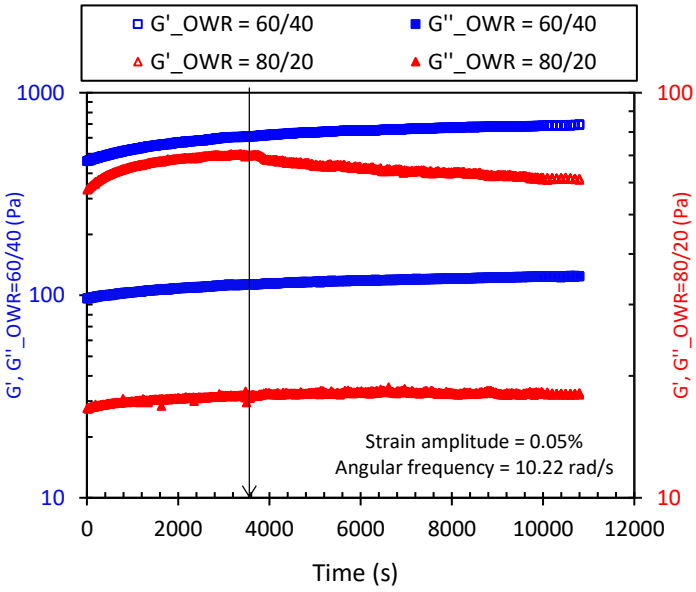

FIGURE 8: Time-dependent oscillatory shear analysis of drilling fluid sample with oil-water ratio (OWR) of 80/20 and 60/40 showing the characteristic profiles of the elastic and viscous moduli in the LVE range of 0.05% and angular frequency of 10.22 rad/s measured at 25°C.

Dynamic Sag Index

In Figure 9, we compared the effects of both rotational shear and oscillatory shear on the dynamic sag index (DSI) for both fluids samples. The criterion for a perfectly stable fluid sample will have DSI equals 0.50. Conditions above this index show the vulnerability of the fluid samples to sag. It is shown from the chart that the fluid sample with OWR = 60/40 sheared under both

rotational and oscillatory conditions revealed very little sag at 10 s^{-1} and almost no sag for the remaining shear rates. However, for fluid sample with OWR = 80/20, rotational shear promoted much sag compared to oscillatory shear particularly at shear rate of 10 s^{-1} It is worth noting that fluid sample with OWR = 60/40 recorded the least sag under both rotational and oscillatory shear conditions due to its stable structural character compared to fluid sample with OWR = 80/20 which showed a less stable structural behavior resulting in high sag.

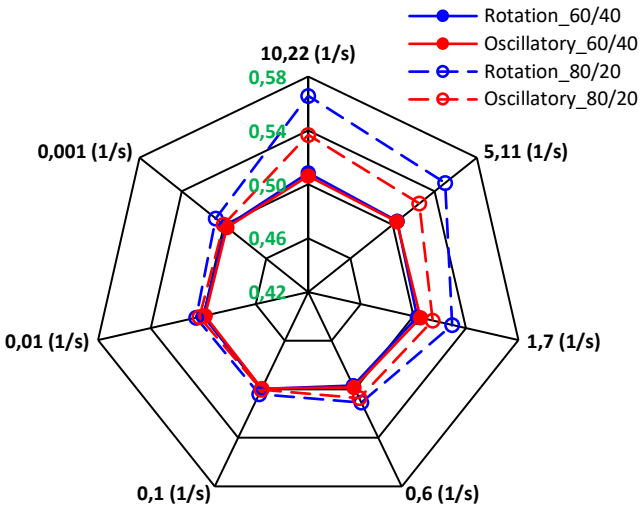

FIGURE 9: Dynamic sag index (DSI) of drilling fluid samples with oil-water ratio (OWR) of 80/20 and 60/40 measured at 25°C and amplitude strain of 0.05%. The vertical scale represents the DSI. The closer the graph to the outer axis, the high the sag potential

In Table 2, we have presented the stability criteria values for the two fluid samples for comparison.

TABLE 2: Comparison of stability criteria values

Stability Criteria	Fluid sample	
	OWR = 80/20	OWR = 60/40
Dynamic yield stress, τ_y (Pa)	0.4	1.4
Static yield stress, τ_s (Pa) @ 0.01s^{-1}, 60s	5	10
Flow transition index, τ_f/τ_y	4.8	5.9
Mechanical storage stability index, MSSI	1.3	1.2
Dynamic sag index, DSI, @ 10.22s^{-1}	0.57	0.51

Case Study: Barite Sag in Well Completion Failure

In the year 1990, an offshore well was completed on a platform in Norway. A tie-back casing string connects to 8-5/8" production through a telescope-joint inside a 13-3/8" intermediate casing. The telescope-joint is used to compensate for temperature and pressure variations. Drilling fluid of 1.9 s.g filled the annulus between the tie-back casing and the intermediate casing. The well produced for about 4 years before a well stimulation operation took place. Then production commence until shut-in for a workover operation 5 years later. Surprisingly, no 9-5/8" casing was present in the wellhead. The casing hanger had been dropped and the top was observed some 5 meters below. A review of operations report indicated that the drop of the 9-5/8" casing hanger took place in 1994 during the well stimulation job. The root cause was barite sag in the drilling fluid causing pack-off and locking of the telescope-joint. By cooling of the tie-back casing during well stimulation, fluid pressure applied on top of the casing hanger and ballooning effect of the casing caused the casing hanger to be forced through the wellhead. Also, the casing hanger design was new and not properly tested in the workshop. Due to this serious event, the well produced with only one pressure barrier in place for about 5 years. Figure 10 illustrates the configuration of the well completion schematic.

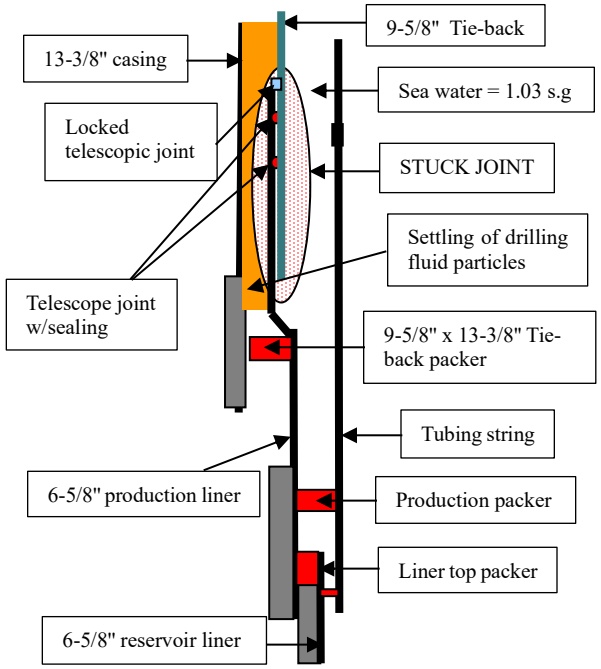

FIGURE 10: Wellbore completion schematics

CONCLUSION

The following can be inferred from this study.

1. The dynamic viscosity of the fluid sample with oil-water ratio (OWR) of 60/40 increased over the entire range of shear rate compared to fluid sample with oil-water ratio of 80/20.
2. In the linear viscoelastic range, the elasticity of the fluid sample with oil-water ratio (OWR) of 60/40 exceeded the fluid sample with oil-water ratio of 80/20 by a factor of 5, indicating a higher storage stability property in the fluid sample with oil-water ratio of 60/40.
3. Both fluid samples show weak gel structures characterized by $G' > G''$ and parallel over the full frequency range. The long-term stability of the fluid sample with oil-water ratio of 60/40 is however higher than that of fluid sample with oil-water ratio of 80/20.

4. Time-dependent oscillatory sweep at rest shows a gel structural growth up to 3600 s for fluid sample with oil-water ratio of 80/20, afterwards, structural breakdown occurs in the fluid sample as evidenced by decrease in G'. There is however a continuous gel buildup in the fluid sample with oil-water ratio of 60/40 over the entire time duration.
5. The static yield stress value of fluid sample with OWR = 80/20 is 5 Pa after 60 s of applied constant shear stress. Likewise, for fluid sample with OWR = 60/40, the static yield stress is 10 Pa after 60 s of applied shear stress. The dynamic yield stress values were several magnitudes less than the static yield stress and calculated as the stress where $G' = 0.9G'_{lin}$.
6. Fluid sample with oil-water ratio of 80/20 promoted much barite sag during both rotational and oscillatory shear as compared to fluid sample with oil-water ratio of 60/40.
7. From the stability criteria, fluid sample with oil-water ratio of 60/40 showed the most stable dispersion with stronger network structure as evidenced by higher yield stress and higher flow transition index values, while lower mechanical storage stability index and lower dynamic sag index values were obtained.

ACKNOWLEDGEMENTS

This work was carried out at the NTNU and SINTEF laboratories. The authors acknowledge the Research Council of Norway and the Norwegian PIRE project partners for financing this study. Special thanks to M-I SWACO, Schlumberger Norge AS for the supply of drilling fluid chemicals and technical support.

REFERENCES

[1] Zamora, M., and Jefferson, D. 1994. "Controlling Barite Sag Can Reduce Drilling Problems", *Oil & Gas Journal* (92) 47-52.

[2] Skalle, P., Backe, K.R., Lyomov, S.K., and Sveen, J. 1999. "Barite Segregation in Inclined Boreholes", *Journal of Canadian Petroleum Technology* (38) 13.

[3] Saasen, A. 2002. Sag of Weight Materials in Oil-Based Drilling Fluids. Presented at the IADC/SPE Asia Pacific Drilling Technology, Jakarta, Indonesia, 9 – 11 September. IADC/SPE 77190. doi:10.2118/77190-MS

[4] Tehrani, A., Zamora, M., and Power, D. 2004. Role of Rheology in Barite Sag in SBM and OBM. Presented at the AADE Drilling Fluids Conference, Houston Texas, 6-7 April.

[5] Jachnik, R.P., and Robinson, G. 2000. "Dynamic Barite Sag in Oil Based Drilling Fluids", *Mineral Processing and Extractive Metallurgy Review*, 20:1, 251-262.

[6] Saasen, A., Liu, D., Marken, C.D. et al. 1995. Prediction of Barite Sag Potential of Drilling Fluids from Rheological Measurements. Presented at the SPE/IADC Drilling Conference, Amsterdam, 28 February – 2 March. SPE 29410-MS. http://dx.doi:10.2118/29410-MS

[7] Dye, W., Hemphill, T., Gusler, W., and Mullen, G. 2001. "Correlation of Ultralow-Shear-Rate Viscosity and Dynamic Barite Sag", *SPE Drilling & Completion* (16) 27-34.

[8] Nguyen, T.C., Miska, S., Saasen, A. and Maxey, J. 2014. "Using Taguchi and ANOVA Methods to Study the Combined Effects of Drilling Parameters on Dynamic Barite Sag", *Journal of Petroleum Science and Engineering*, 121, 126-133.

[9] Nguyen, T., Miska, S., Yu, M., Takach, N., Ahmed, R., Saasen, A., Omland, T.H. and Maxey, J. 2011. "Experimental Study of Dynamic Barite Sag in Oil-Based Drilling Fluids using a Modified Rotational Viscometer and a Flow Loop", *Journal of Petroleum Science and Engineering*, **78**, 160-165.

[10] Massam, J., Popplestone, A.,and Burn, A. 2004. A Unique Technical Solution to Barite Sag in Drilling Fluids. Presented at the AADE 2004 Drilling Fluid Conference, Houston, Texas, 6 – 7 April. AADE-04-DF-HO-21

[11] Tehrani, A. 2007. "Behaviour of Suspensions and Emulsions in Drilling Fluids", *Annual Transactions of the Nordic Rheology Society*, Vol 15, 1-9.

[12] Maxey, J. 2007. "Rheological Analysis of Static and Dynamic Sag in Drilling Fluids", *Annual Transactions of the Nordic Rheology Society* Vol. 15, 181-188.

[13] Elkatatny, S. 2018. "Enhancing the Stability of Invert Emulsion Drilling Fluid for Drilling in High-Pressure High-Temperature Conditions", *Energies*, 11, 2393.

[14] Mohamed, A., Basfar, S., Elkatatny, S., Al-Majed, A. 2019. "Prevention of Barite Sag in Oil-Based Drilling Fluids Using a Mixture of Barite and Ilmenite as Weighting Material", *Sustainability*, *11*, 5617.

[15] Bokern, D.G., Hunter, K.A., McGrath, K.M. 2003. "Charged Barite – Aqueous Solution Interface: Surface Potential and Atomically Resolved Visualization", *Langmuir*, 19, 10019-10027.

[16] Belayneh, M., Aadnøy, B.S., and Thomas, S. 2016. Dynamic and Static Sagging Characterization and Performances of Four Oil Based Muds. Presented at the ASME 2016 35th International Conference on Ocean, Offshore and Arctic Engineering, OMAE2016-54457.

[17] Kulkarni, S.D, Savari, S., Gantepla, A., Murphy, R., Jamison, D., Tonmukayakul, N., and Teke, K. 2013. Visco-Elastic Settling Rate Models to Determine Sag Potential of Non-Aqueous Drilling Fluids. Presented at the AADE National Technical Conference and Exhibition, Cox Convention Centre, Oklahoma City, February 26-27, AADE-13-FTCE-26.

[18] Savari, S., Kulkarni, S., Maxey, J., and Teke, K. 2013. A Comprehensive Approach to Barite Sag Analysis on Field Muds. AADE National Technical Conference and Exhibition, Cox Convention Centre, Oklahoma City, February 26-27, AADE-13-FTCE-30.

[19] Ofei, T.N., Lund, B., Saasen, A., Sangesland, S., Gyland, K.R., and Linga, H. 2019. "A New Approach to Dynamic Barite Sag Analysis on Typical Field Oil-Based Drilling Fluid", *Annual Transactions of the Nordic Rheology Society*, Vol. 27, 61-69.

[20] Maxey, J. 2006. Rheological Analysis of Oilfield Drilling Fluids. Presented at the AADE 2006 Fluids Conference, Houston, Texas, 11 – 12 April. AADE-06-DF-HO-01.

[21] Mullen, G., Perez, J., Dye, B.,and Gusler, B. 2003. Coupling of Technologies for Concurrent ECD and Barite Sag Management. Presented at the AADE 2003 National Technology Conference "Practical Solutions for Drilling Challenges", Houston, Texas, 1 – 3 April. AADE-03-NTCE-29

[22] Mezger, T.G. 2014. The Rheology Handbook. 4ed. Vincentz Network, Hannover, Germany.

[23] Hold, S. 2015. "The Very Basics of Density Measurement Methods", Anton Paar Blog. https://blog.anton-paar.com/the-very-basics-of-density-measurement/.20/10/19.

[24] Douglas, J.F. 2018. "Weak and Strong Gels and the Emergence of the Amorphous Solid State", *Gels*, 4, 19, 1-14.